Eddy Effects in the General Circulation, Spanning Mean Currents, Mesoscale Eddies, and Topographic Generation, Including Submesoscale Nests

Alexander F. Shchepetkin (PI)
James C. McWilliams and Maarten J. Molemaker (Co-PIs)
Department of Atmospheric and Oceanic Sciences
University of California, Los Angeles, CA 90095-1565
phone:(310)206-9381 fax:(310)206-5219 email:alex@atmos.ucla.edu

N00014-12-1-0939
http://www.atmos.ucla.edu/roms/

LONG-TERM GOALS

Our goals are the continuing development of the Regional Oceanic Modeling System (ROMS) with emphasis on the ability to simulate realistic, highly-turbulent flows at basin, regional, and local scales at resolutions sufficient to capture submesoscale phenomena through the use of grid nesting techniques; analysis and understanding the underlying physical processes; and improved parameterizations of unresolved processes, applicable numerical algorithms, and relevant computer-science techniques needed for an efficient parallel code adapted for modern computing environments

OBJECTIVES

The central scientific questions are how the eddies control the persistent currents by their eddy-induced momentum and buoyancy fluxes, turbulent mixing, and their bottom form stress (pressure force) and bottom boundary layers – all the aspects associated with turbulent flows over steep topography in the presence of stratification. These questions are investigated in the context of western boundary currents, the Gulf Stream and the Kuroshio, as well as the western Pacific (Solomon Sea). The intent is obtain realistically accurate separation and the subsequent path of the Gulf Stream, the Kuroshio path from Taiwan to Japan with subsequent separation, as well as provide analysis of modeling sensitivities to input parameters and forcing, and, wherever possible, to understand and give a physical explanation of the underlying mechanisms. This involves validation against real-world data in cooperation with William S. Kessler and Hristina Hristova from PMEL (Solomon Sea), and Satoshi Mitarai and Taichi Sakagami from Okinawa Institute of Science and Technology (Kuroshio).

APPROACH

The primary method is to obtain numerical solutions on sets of progressively refined grids, starting with basin-wide eddy permitting resolutions (although substantially finer than that used in climate modeling), and downscaling it to $\Delta x \sim 1km$ or less, which enables adequate resolution of mesoscale and submesoscale eddies generated by instability and bottom topography effects. This is accompanied by development of modeling codes, numerical methods, and the associated pre- and post-processing infrastructure, analysis, and visualization that allows prioritizing the tasks directly necessary for achieving the objectives stated above, but, at the same time, traditionally maintaining

Report Documentation Page

Form Approved
OMB No. 0704-0188

1. REPORT DATE	2. REPORT TYPE	3. DATES COVERED
30 SEP 2014		**00-00-2014 to 00-00-2014**

4. TITLE AND SUBTITLE	5a. CONTRACT NUMBER
Eddy Effects in the General Circulation, Spanning Mean Currents, Mesoscale Eddies, and Topographic Generation, Including Submesoscale Nests	5b. GRANT NUMBER
	5c. PROGRAM ELEMENT NUMBER
6. AUTHOR(S)	5d. PROJECT NUMBER
	5e. TASK NUMBER
	5f. WORK UNIT NUMBER
7. PERFORMING ORGANIZATION NAME(S) AND ADDRESS(ES) **University of California, Los Angeles,Department of Atmospheric and Oceanic Sciences,Los Angeles,CA,90095**	8. PERFORMING ORGANIZATION REPORT NUMBER
9. SPONSORING/MONITORING AGENCY NAME(S) AND ADDRESS(ES)	10. SPONSOR/MONITOR'S ACRONYM(S)
	11. SPONSOR/MONITOR'S REPORT NUMBER(S)

12. DISTRIBUTION/AVAILABILITY STATEMENT
Approved for public release; distribution unlimited

13. SUPPLEMENTARY NOTES

14. ABSTRACT

15. SUBJECT TERMS

16. SECURITY CLASSIFICATION OF:			17. LIMITATION OF ABSTRACT	18. NUMBER OF PAGES	19a. NAME OF RESPONSIBLE PERSON
a. REPORT **unclassified**	b. ABSTRACT **unclassified**	c. THIS PAGE **unclassified**	**Same as Report (SAR)**	**19**	

the 3-way balance among physical applications (including introducing new submodels), numerical methods, and computer science that has been established throughout ROMS development history. Additionally, we design idealized, process-study-oriented simulations with the intent of understanding of physical phenomena, and as control tests for algorithm verification.

WORK COMPLETED

During the last year we worked on decadal Pacific and Atlantic circulations, the Kuroshio, and the Gulf Stream; mesoscale eddy buoyancy fluxes; submesoscale surface fronts, filaments, and eddies; topographic current separation, form stress, and submesoscale vortex generation. Our work on isoneutral diffusion for tracers is now published (Lemarié, *et al.*, 2012a,b); however, recently we have revisited the relevant parts of the code with the intents of reducing its computational cost and for better integrating its algorithm with the rest of the model. For new algorithms we implemented adaptively implicit vertical advection to alleviate the associated CFL limitations, which has been a growing impediment for high-resolution simulations, especially in shallow water and for modeling tides. The code now utilizes dual (shared- and distributed-memory) parallelization (implemented via Open MP and MPI, respectively, with an option to use both at the same time) based on subdomain decomposition for both with two-level hierarchy. We also made an effort to parallelize pre-processing software tools wherever justified by their computational cost. A substantial effort on improved analysis and visualization techniques that involves a transition from Matlab to Python-based software and graphics was made by Jonathan Gula.

RESULTS

We present a few highlights for this project. The annual publication list (papers from 2013 through those submitted so far in 2014) provides a view of the finalized results across all our ONR modeling projects.

Adaptive, Courant-Number-Dependent Implicit Vertical Advection: This work was partly reported last year. It is now in a mature stage: Shchepetkin (2104) was submitted and has passed one review round. The approach is to monitor Courant numbers at each time step and each grid point, and split vertical velocity into two parts: one is to be treated in the conventional explicit time-stepping way, and the remaining part (essentially "excess") becomes a part of the implicit solver. This applies for both momentum and tracer equations. The implicit advection part is deliberately designed to be dissipative to prevent dispersive oscillations in a super-Courant regime, while the adaptability is optimized to stay explicit as much as possible. While the algorithm may seem to be mathematically complex, it integrates naturally into the existing code structure, resulting in no new subroutines, synchronization points, or message passing events added into the code, thus incurring only a modest increase in computational cost, well offset by the gains in improved stability and robustness.

To illustrate its effect on a realistic simulation, we re-ran one of our problems of interest, the Northwestern Atlantic nested Gulf Stream area configuration using the adaptive code (***n.b.,*** this is the same subdomain as the outer box in Fig. 5 below). The upper-left panel of Fig. 1 shows the model domain and topography. Grid resolution is $\Delta x = 750$-meter with $1200 \times 1400 \times 50$ grid points. The time step is $\Delta t = 90s$ for the adaptive code, which is at least double of what we were able to run without adaptability. The total duration of the run is in excess of 33 model months. The open boundaries are forced by data interpolated from a coarse resolution run covering a larger area by the Mason *et al.*(2010) technique. The two right panels of Fig. 1 show a snapshot of vertical maxima of

the instantaneous horizontal, c_x, and vertical, c_w, Courant numbers, which must be bounded for stable time-stepping with explicit schemes. While the horizontal c_x achieves the "healthy" values of 0.5 (*i.e.,* stable and nearly optimal), the vertical c_w are very small almost everywhere except at a very few points barely noticeable on this plot (*n.b.,* the pixel resolution in these figures is only one pixel per two grid points in each direction, thus involving 4-point averaging; also notice the stretched colorbar on the c_w panel). Nevertheless, it is c_w that is the most restrictive factor in setting the maximum time-step in this run.

Figure 2 shows the maxima of c_x and c_w over nearly the whole 33 months of model integration with temporal samples every 12 hours (*i.e.,* 1990 individual snapshots). While Fig. 2 does not provide sufficient pixel resolution to diagnose individual "hot spots", it does show the overall pattern of where to expect them. Figures 3 and 4 provide further detail. One generic location for large c_w is in very shallow water, with very small vertical grid spacing Δz, steep topographic slope, and sharp contrasts in density due to high nearshore salinity anomalies; the horizontal currents are not particularly intense in this area. Another such location is near the shelf-break that is known to be a site of strong vertical velocity due to tides and eddies. On both of these latter figures the individual grid boxes of horizontal grid are pixel-resolved, thus allowing us to fully examine the maximum values. It should be noted that with the adaptive vertical advection algorithm, this computational regime (*i.e.,* time-step, grid resolution, topography, and flow intensity) is beyond the capability of the previous explicit-advection code.

Dynamical Balance of the Mean Gulf Stream: Identifying the dynamics responsible for the Gulf Stream separation and the control of its path has been a long-standing challenge in oceanography. The dynamical balance of the Gulf Stream is investigated using very high-resolution ROMS simulations highlighting the important role played by eddy-driven flows and the interactions with complex topography. The Gulf Stream strongly interacts with the topography along the Southeastern U.S. Seaboard, between the Straits of Florida and Cape Hatteras. The dynamics of the Gulf Stream in this region has been investigated with a set of realistic, very high resolution simulations using the oceanic model ROMS (Fig. 5). The mean path is strongly influenced by the topography and in particular the Charleston Bump. There are significant local pressure anomalies and topographic form stresses exerted by the Bump that retard the mean flow and steer the mean current pathway seaward (Fig. 6). The effect of the topography on the development of meanders and eddies has been studied by computing energy budgets of the eddies and the mean flow. The baroclinic instability is stabilized by the slope everywhere except past the Bump. The flow is barotropically unstable, and kinetic energy is converted from the mean flow to the eddies following the Straits of Florida and at the Bump with regions of eddy-to-mean conversion in-between. The pattern of eddy fluxes is interpreted in terms of eddy life cycle; eddy fluxes are directed down-gradient in eddy growth regions and up-gradient in eddy decay regions.

By revisiting the classic gyre equilibrium problem, the dominant role of bottom pressure torque in the closure of the gyre scale barotropic vorticity budget has been established. The bottom pressure torque is the term balancing the negative input by anticyclonic wind curl on the scale of the subtropical gyre. The bottom pressure torque, which is derived from the twisting of the force that bottom topography exerts on the ocean, is the main ingredient enabling the return flow of the wind-driven transport in western boundary currents. The meridional transport of fluid is balanced by the sum of the bottom pressure torque and the non-linear advective term. The non-linear advective term redistributes vorticity locally, but the bottom pressure torque is the term providing the overall positive input of vorticity, balancing the negative input by anticyclonic wind curl on the scale of the subtropical gyre

(Fig. 7). The Gulf Stream path is directly linked to the bottom pressure torque and its related eddy-driven abyssal circulation. There is a relation between the abyssal currents and the bottom pressure torque (as expected from the relation $-f\vec{u_b}.\vec{\nabla}h = \frac{\mathbf{J}(P_b,h)}{\rho_0}$ for a geostrophic current) that translates into bottom vortex stretching and controls the Gulf Stream path southward deflections. This is how the abyssal circulation and, in particular, the Deep Western Boundary Current (DWBC) play a role in the Gulf Stream path and separation. The path and the transport of the Gulf Stream are also controlled by the intensity of the two eddy-driven recirculation gyres north and south of the flow. Vorticity balance for the two recirculation gyres shows that they are driven by advective fluxes, while the bottom drag is the main sink of vorticity for both gyres; this term is positive for the anticyclonic gyre and negative for the cyclonic one.

Western Boundary Current, Mesoscale Eddies, and Submesoscale Flow in the Southwest Pacific Sea: A high-resolution (dx = 4 km) climatologically-forced ocean model, validated by altimetry and glider data, is used to characterize the vertical and seasonal variations of mesoscale variability in the Solomon and Coral Seas (Fig. 8). The highest eddy kinetic energy (EKE) in the southwest Pacific is found subsurface in the Gulf of Papua, at the depth of the low-latitude western boundary current velocity core. Variability associated with the western boundary current, especially downstream of topographic obstacles, dominates the thermocline and intermediate level EKE. By contrast, surface EKE is generally enhanced in the southwest Pacific with a pronounced annual cycle that has a phase difference between small-scale and large-scale variability. Large mesoscale eddies account for most of the surface EKE and its annual modulation. The June maximum of surface EKE in the Solomon Sea, and the December maximum in the Coral Sea can be accounted for by local instabilities of large-scale currents. Small mesoscale eddies, predominantly cyclonic, are abundant in late winter (AugustSeptember), coinciding with the timing of deepest mixed layer and strongest vertical velocity. They contribute to the spatially-uniform surface-enhanced EKE over the top 100 m, not associated with the western boundary current. In the Coral Sea, small mesoscale eddies are generated mostly by open-ocean surface baroclinic instabilities, while in the land-bounded Solomon Sea near-boundary barotropic instabilities and topographic generation are also important. This is reported in Hristova *et al.* (2014).

A higher-resolution (dx = 1.5 km) nested solution is used to characterize the circulation and the topographic interactions of the Southwest Pacific, including the Solomon and Coral Seas and the Gulf of Papua New Guinea. As illustrated in Fig. 9, those regions are characterized by the presence of the New Guinea Western Boundary Current that becomes violently unstable when flowing around the Louisiades Peninsula, out of the Gulf of Papua New Guinea and into the Solomon Sea. It induces sharp fronts, filaments, and coherent vortices through topographic interactions. The turbulent submesoscale activity is further increased by the strong vorticity generation in the boundary layer along the complex topography of the Solomon Sea. The Coral Sea is less impacted by the presence of the Western Boundary Current and can be classified as a classic submesoscale surface boundary layer instabilities regime that is likely created by mesoscale strain fields that explosively sharpens lateral buoyancy gradients, which in turn become highly unstable (McWilliams *et al.*, 2009a, 2009b, 2010). These structures catalyze energy dissipation for the large-scale circulation and are responsible for a large part of the vertical fluxes of mass, buoyancy, and other materials in the upper oceanic layers. A manuscript on Solomon Sea submesoscale structure is being prepared.

Influence of the Coastal Wind Profile on Circulation and Primary Production off the U.S. West Coast: The Californian Current System (CCS) is an Eastern Boundary Upwelling System (EBUS), which are among the most productive marine ecosystems in the world supporting major fisheries (*e.g.,* FAO

2009). Its cold and productive water is largely determined by wind-driven upwelling. The CCS upwelling presents a seasonal variability with a favorable season during spring and summer (*e.g.,* Marchesiello *et al.*, 2003). A cross-shore pressure gradient between the North Pacific High and the Continental Thermal Low pressure systems (Huyer *et al.*, 1983) leads to dominant alongshore winds favoring upwelling circulation. As for the other EBUS (*e.g.,* Humboldt, Benguela, and Canary Currents), equatorward winds drive alongshore currents, Ekman-induced upwelling, cross-shore exchange, and productivity. The spatial structure and amplitude of these phenomena depend on the shape of the coastal winds as they transition from strong over the ocean to weaker over land due to differences in surface drag; however, this transition zone is poorly measured in its low-frequency wind structure. We demonstrate this sensitivity by using alternative wind forcing fields. A coupled biogeochemical and physical simulation (with a grid scale of $dx = 4$ km) is carried out to assess the control of the local wind profiles on the circulation and Primary Production (PP) off the U.S. West Coast. Three experiments have been carried out using the very same forcing from QuikSCAT, but a different wind profile resulting in a different wind drop-off widths in the extrapolation toward the shoreline (where the scatterometer is blind): wide, sharp, or no drop-off. With different drop-offs the poleward Undercurrent has different transports and, sometimes, even a reversed surface current (Fig. 10). Using a Nitrate budget analysis, we show the Nitrate reservoir depends on the coastal wind profiles through changes in the vertical and horizontal advection rates. In particular, although the along- and cross-shore integrated vertical velocities remain the same in the different experiments, the cross-shore integrated Nitrate is not conserved when changing the drop-off length (Fig. 11). As a result, as illustrated in Fig. 12, during Spring between 35N and 40N, the Primary Production (PP) can be doubled by changing the coastal wind profile. This implies that conventional upwelling indices related to broad features of the wind are not accurate to predict the PP related to upwelling. This demonstrates both the importance of spatially detailed wind forcing (*i.e.,* better than available from satellites or global reanalyses) and an implication of a recalcitrant modeling uncertainty insofar as such detailed winds might not routinely be available.

IMPACT/APPLICATIONS

Geochemistry and Ecosystems: An important community use for ROMS is biogeochemisty: chemical cycles, water quality, blooms, micro-nutrients, larval dispersal, biome transitions, and coupling to higher tropic levels. We collaborate with Profs. Keith Stolzenbach (UCLA), Curtis Deutsch (UCLA), David Siegel (UCSB), and Yusuke Uchiyama (Kobe).

Data Assimilation: We collaborate with Dr. Zhinjin Li (JPL) and Prof. Kayo Ide (U. Maryland) by developing model configurations for targeted regions and by consulting on the data-assimilation system design and performance. Current quasi-operational, 3DVar applications are in California (SCCOOS and CenCOOS) and in Alaska (Prince William Sound).

TRANSITIONS

The ROMS modeling codes of UCLA and associated supporting software are generally available as open source. We also made available some of our solutions for the analysis by third parties. ROMS is a community code with widespread applications (http://www.myroms.org).

RELATED PROJECTS

Wave-current interaction (in cooperation with Yusuke Uchiyama, University of Kobe, Japan); biogeochemical modeling (in cooperation with Curtis Deutsch, Jun-Hong Liang, and Hartmut Frenzel, University of Washington); and data assimilation analyses and forecasts in the Integrated Ocean Observing System (IOOS) regional projects for California and Alaska (SCCOOS, CenCOOS, and AOOS).

REFERENCES

Food and Agriculture Organization of the United Nations (FAO), 2009: *State of the World's Fisheries and Aquaculture 2008*, Rome.

Huyer, A., 1983: Coastal upwelling in the California Current System. *Prog. Oceanography* **12**, 259-284.

Lemarié, F., J. Kurian, A.F. Shchepetkin, M.J. Molemaker, F. Colas, and J.C. McWilliams, 2012a: Are there inescapable issues prohibiting the use of terrain-following coordinates in climate models? *Ocean Modelling* **42**, 57-79. [published, refereed]

Lemarié, F., L. Debreu, L., A.F. Shchepetkin, and J.C. McWilliams, 2012b: On the stability and accuracy of the harmonic and biharmonic adiabatic mixing operators in ocean models. *Ocean Modelling* **52-53**, 9-35. [published, refereed]

Mason, E., M.J. Molemaker, A. F. Shchepetkin, F. Colas, J.C. McWilliams, and P. Sangrà, 2010: Procedures for offline grid nesting in regional ocean models. *Ocean Modelling* **35**, 1-15.

Marchesiello, P., J.C. McWilliams, & A. Shchepetkin, 2003: Equilibrium structure and dynamics of the California Current System, *J. Phys. Ocean.* **33**, 753-783.

McWilliams, J.C., M.J. Molemaker, & E.I. Olafsdottir, 2009a: Linear fluctuation growth during frontogenesis. *J. Phys. Ocean.* **39**, 3111-3129.

McWilliams, J.C., F. Colas, & M.J. Molemaker, 2009b: Cold filamentary intensification and oceanic surface convergence lines. *Geophys. Res. Lett.* **36**, L18602.

McWilliams, J.C., 2010: A perspective on submesoscale geophysical turbulence. In: *IUTAM Symposium on Turbulence in the Atmosphere and Oceans*, D. Dritschel, ed., Springer, 131-141.

PUBLICATIONS

Bracco, A., J.D. Neelin, H. Luo, J.C. McWilliams, and J.E. Meyerson, 2013: High dimensional decision dilemmas in climate models. *Geosci. Model Dev.*, **6**, 2731-2767. [published, refereed]

Colas, F., X. Capet, J.C. McWilliams, and Z. Li, 2013a: Mesoscale eddy buoyancy flux and eddy-induced circulation in eastern boundary currents. *J. Phys. Ocean.*, **43**, 1073-1095.

[published, refereed]

Colas, F., X. Wang, X. Capet, Y. Chao, and J.C. McWilliams, 2013b: Untangling the roles of wind, run-off and tides in Prince William Sound. *Continen. Shelf Res.*, **63**, S79-S89. [published, refereed]

Dewar, W.K., J.C. McWilliams, and M.J. Molemaker, 2014: Centrifugal instability and mixing in the California Undercurrent. *J. Phys. Ocean.*. [submitted]

Dong, C., J.C. McWilliams, Y. Liu, & D. Chen, 2014: Global heat and salt transports by eddy movement. *Nature Geosci.*. [in press]

Farrara, J., Y. Chao, Z. Li, X. Wang, X. Jin, H. Zhang, P. Li, Q. Vu, P. Olsson, C. Schoch, M. Halverson, M. Moline, C. Ohlmann, M. Johnson, J.C. McWilliams, and F. Colas, 2013: A data-assimilative ocean forecasting system for the Prince William Sound and an evaluation of its performance during Sound Predictions 2009. *Continen. Shelf Res.*, **63**, S193-S208. [published, refereed]

Gula. J., M. J. Molemaker, and J. C. McWilliams, 2013a: Gulf Stream dynamics and frontal eddies along the Southeast U.S. continental shelf. *J. Phys. Ocean.* [submitted]

Gula. J., M. J. Molemaker, and J. C. McWilliams, 2013b: Submesoscale cold filaments in the Gulf Stream. *J. Phys. Ocean.*. [in press]

Hristova, H., W.S. Kessler, J.C. McWilliams, and M.J. Molemaker, 2014: Eddy distribution and seasonality in the Solomon and Coral Seas. *J. Geophys. Res.*. [in press]

Kumar, N., F. Feddersen, Y. Uchiyama, J. McWilliams, and W. O'Reilly, 2014: Mid-shelf to surf zone coupled ROMS-SWAN model-data comparision of waves, currents, and temperature: Diagnosis of subtidal forcings and response. *J. Phys. Ocean*. [submitted]

Li, Z., Y. Chao, J. Farrara, and J.C. McWilliams, 2013: Impacts of distinct observations during the 2009 Prince William Sound field experiment: A data assimilation study. *Continen. Shelf Res.*, **63**, S209-S222. [published, refereed]

Li, Z., Y. Chao, J. McWilliams, K. Ide, and J.D. Farrara, 2014: Coastal ocean data assimilation using a multi-scale three-dimensional variational scheme. *Q. J. Roy. Met. Soc.*. [submitted]

Liang, J.-H., C. Deutsch, J.C. McWilliams, B. Baschek, P.P. Sullivan, and D. Chiba, 2013: Parameterizing bubble-mediated air-sea gas exchange and its effect on ocean ventilation. *Glob. Biogeo. Cycles*, **27**, 894-905. [published, refereed]

Marchesiello, P. R. Benshilat, R. Almar, Y. Uchiyama, J. McWilliams, and A. Shchepetkin, 2014: On tridimensional rip current modeling. *Ocean Modelling*. [submitted]

Mason, E., A. Pascual, and J.C. McWilliams, 2014: A new sea surface height based code for oceanic mesoscale eddy tracking. *J. Ocean. Atmos. Tech.* **31**, 1181-1188. [published, refereed]

McWilliams, J.C., and B. Fox-Kemper, 2013: Oceanic Wave-balanced surface fronts and filaments. *J. Fluid Mech.*, **730**, 464-490. [published, refereed]

McWilliams, J.C., J. Gula, M.J. Molemaker, L. Renault, and A.F. Shchepetkin, 2014: Filament frontogenesis by boundary layer turbulence. *J. Phys. Ocean.* [submitted]

McWilliams, J.C., E. Huckle, J. Liang, and P.P. Sullivan, 2014: Langmuir Turbulence in swell. *J. Phys. Ocean.*, **44**, 870-890. [published, refereed]

Mechoso, C. R., R. Wood, R. Weller, C.S. Bretherton, A.D. Clarke, H. Coe, C. Fairall, J.T. Farrar, G. Feingold, R. Garreaud, C. Grados, J. McWilliams, S.P. de Szoeke, S.E. Yuter, and P. Zuidema, 2014: Ocean-Cloud-Atmosphere-Land Interactions in the Southeastern Pacific: The VOCALS Program. *Bull. Amer. Met. Soc.*. [in press]

Molemaker, M. J., J.C. McWilliams, and W.K. Dewar, 2014: Submesoscale instability and generation of mesoscale anticyclones near a separation of the California Undercurrent. *J. Phys. Ocean.*. [submitted]

Molemaker, M.J., J.C. McWilliams, and W.K. Dewar, 2013: Centrifugal instability and mixing in the California Undercurrent. *J. Phys. Ocean.* [submitted]

Romero, L., Y. Uchiyama, J.C. Ohlmann, J.C. McWilliams, and D.A. Siegel, 2013: Simulations of nearshore particle-pair dispersion in Southern California *J. Phys. Ocean.*, **43**, 1862-1879. [published, refereed]

Shchepetkin, A.F., 2014: An adaptive, Courant-number-dependent implicit scheme for vertical advection in oceanic models. *Ocean Modelling*, submitted.

Shcherbina, A.Y., E.A. D'Asaro, C.M. Lee, J.M. Klymak, M.J. Molemaker, and J.C. McWilliams, 2013: Statistics of vertical vorticity, divergence, and strain in a developed submesoscale turbulence field. *Geophys. Res. Lett.*, **40**, 4706-4711. [published, refereed]

Shcherbina, A.Y., Miles A. Sundermeyer, Eric Kunze, Eric DAsaro, Gualtiero Badin, Daniel Birch, Anne-Marie E. G. Brunner-Suzuki, Jrn Callies, Brandy T. Cervantes, Mariona Claret, Brian Concannon, Jeffrey Early, Raffaele Ferrari, Louis Goodman, Ramsey R. Harcourt, Jody M. Klymak, Craig M. Lee, M.-Pascale Lelong, Murray D. Levine, Ren-Chieh Lien, Amala Mahadevan, James C. McWilliams, M. Jeroen Molemaker, Sonaljit Mukherjee, Jonathan D. Nash, Tamay zgkmen, Stephen D. Pierce, Sanjiv Ramachandran, Roger M. Samelson, Thomas B. Sanford, R. Kipp Shearman, Eric D. Skyllingstad, K. Shafer Smith, Amit Tandon, John R. Taylor, Eugene A. Terray, Leif N. Thomas, and James R Ledwell, 2014: TheLatMix Summer Campaign: Stirring in the Upper Ocean. *Bull. Amer. Met. Soc.*. [submitted]

Sullivan, P.P., J.C. McWilliams, and E.G. Patton, 2014: Large eddy simulation model of the marine atmospheric boundary layer above a spectrum of moving waves. *J. Atmos. Sci.*. [in press]

Uchiyama, Y., E. Idica, J.C. McWilliams, and K. Stolzenbach, 2013: Wastewater effluent dispersal in two Southern California Bays. *Continen. Shelf Res.*, **76**, 36-52. [published, refereed]

Wang, P., J.C. McWilliams, and C. Ménesguen, 2013: Ageostrophic instability in rotating, stratified interior vertical shear flows. *J. Fluid Mech.*, **755**, 397-428. [published, refereed]

Wang, X., Y. Chao, H. Zhang, J. Farrara, Z. Li, X. Jin, K. Park, F. Colas, J.C. McWilliams, C. Paternostro. C.K. Shum, Y. Yi, C. Schoch, and P. Olsson, 2013: Modeling tides and their influence on the circulation in Prince William Sound, Alaska. *Continen. Shelf Res.*, **63**, S126-S137. [published, refereed]

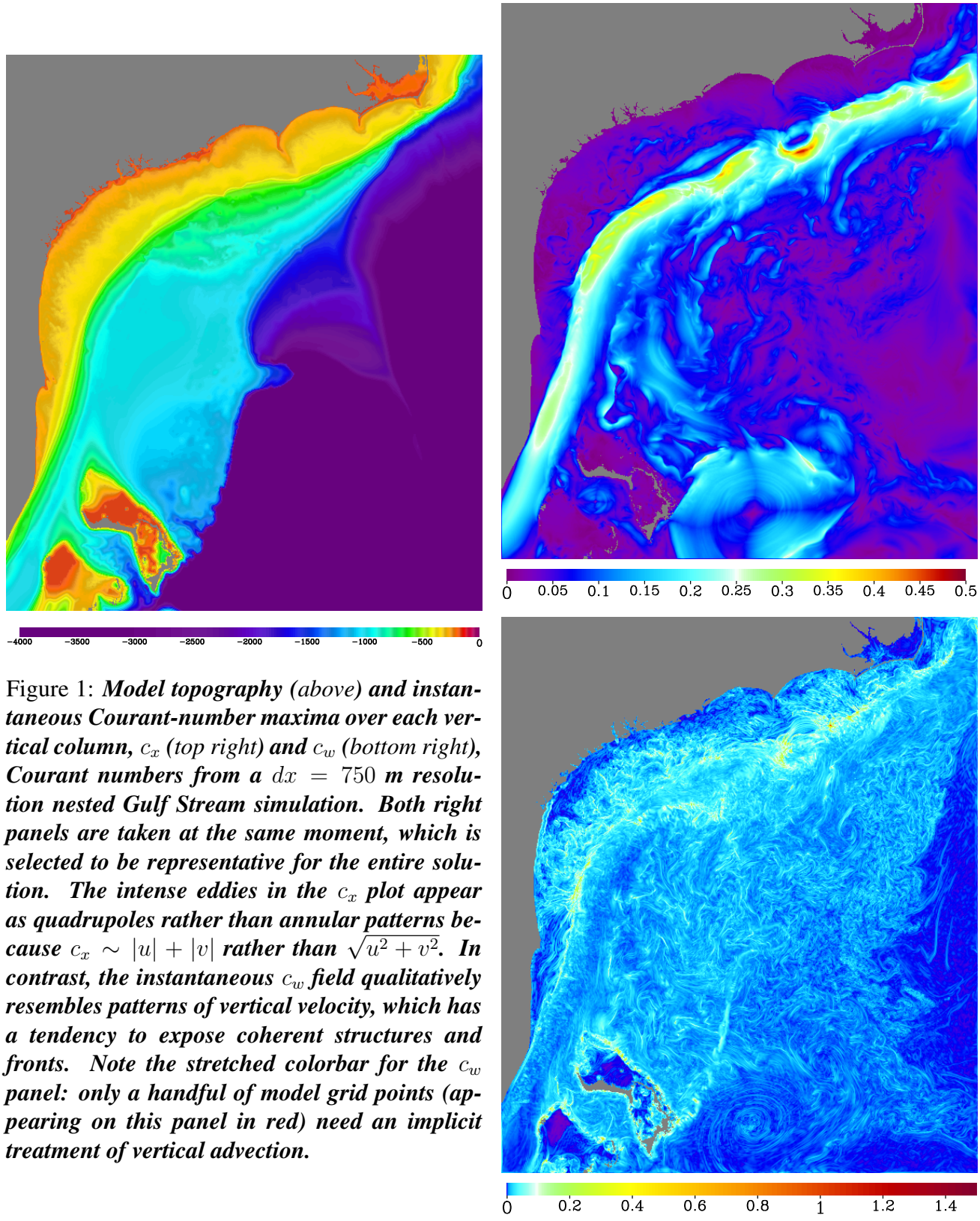

Figure 1: ***Model topography** (above) **and instantaneous Courant-number maxima over each vertical column,** c_x **(top right) and** c_w **(bottom right), Courant numbers from a** $dx = 750$ **m resolution nested Gulf Stream simulation. Both right panels are taken at the same moment, which is selected to be representative for the entire solution. The intense eddies in the** c_x **plot appear as quadrupoles rather than annular patterns because** $c_x \sim |u| + |v|$ **rather than** $\sqrt{u^2 + v^2}$**. In contrast, the instantaneous** c_w **field qualitatively resembles patterns of vertical velocity, which has a tendency to expose coherent structures and fronts. Note the stretched colorbar for the** c_w **panel: only a handful of model grid points (appearing on this panel in red) need an implicit treatment of vertical advection.***

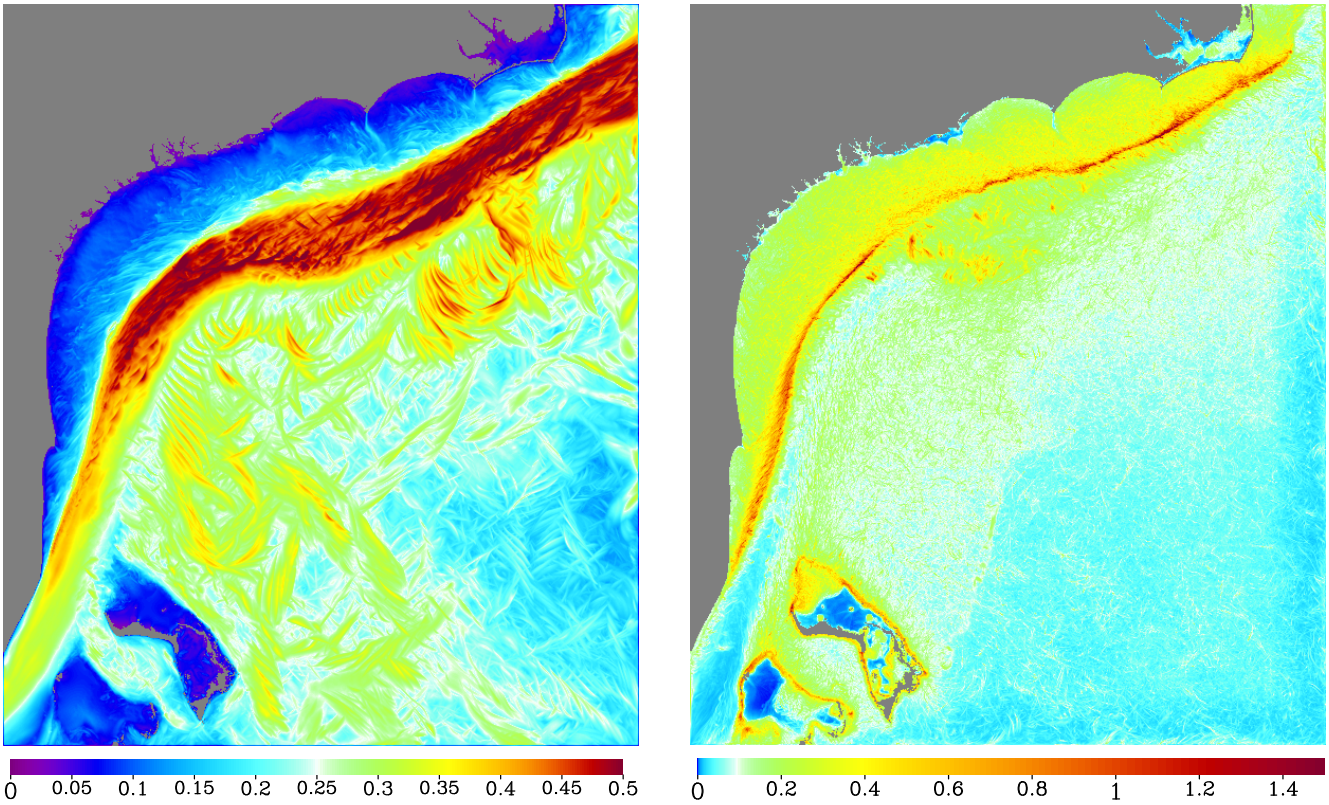

Figure 2: ***Maximum values of maxima over each vertical column and the entire model run of horizontal,*** c_x *(left)****, and vertical*** c_w *(right)****, Courant numbers from the the solution in Fig. 1. Unlike the corresponding*** c_w ***panel on Fig. 1, which does not show evident correlation with model topography, this time it does, and the*** c_w ***panel can be interpreted as the map of "hot spots," which flags the most challenging locations for computational stability on the model grid and topography.***

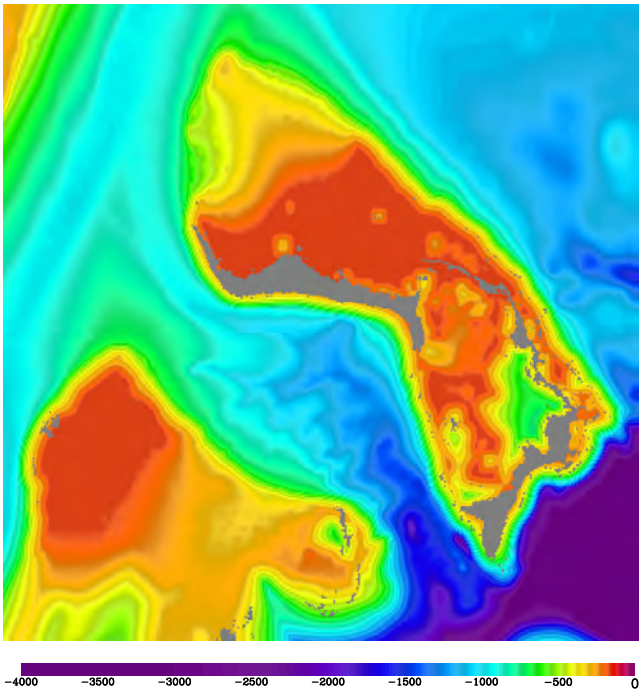

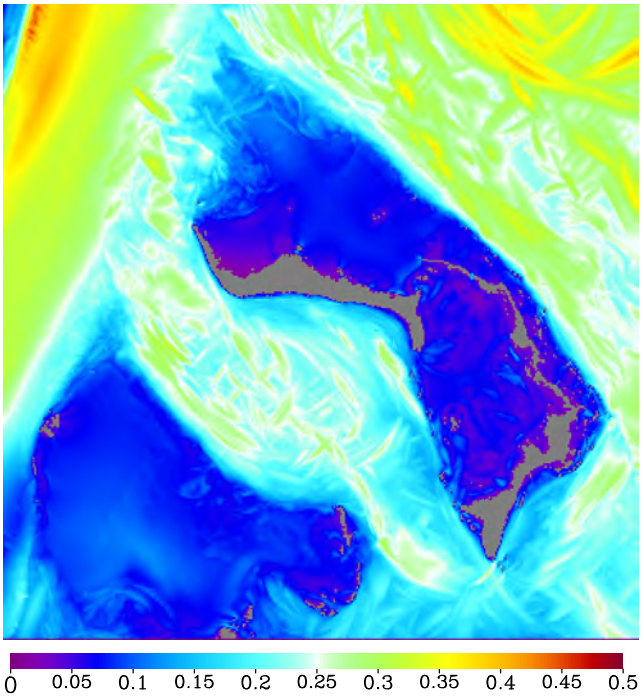

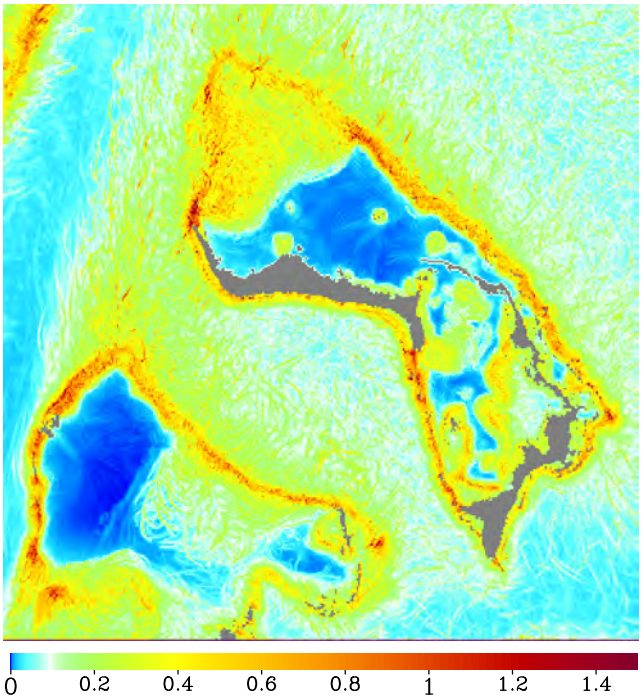

Figure 3: ***An enlarged portion in southwestern corner of Fig. 2. At this location the c_x are too small to pose any concern about numerical stability; however, the c_w are very restrictive. Note the persistent "hot spot" just past the western tip of Grand Bahama Island. This is explained by relatively stagnant water in the shallow area north from Grand Bahama, which is shielded from Gulf Stream influence and tends to generate a high salinity anomaly due to persistent evaporation and lack of exchange. Once the flow separates from the western tip, it creates a front with a large horizontal salinity contrast, resulting in a geostrophic adjustment and frontal secondary circulation with intense vertical velocity.***

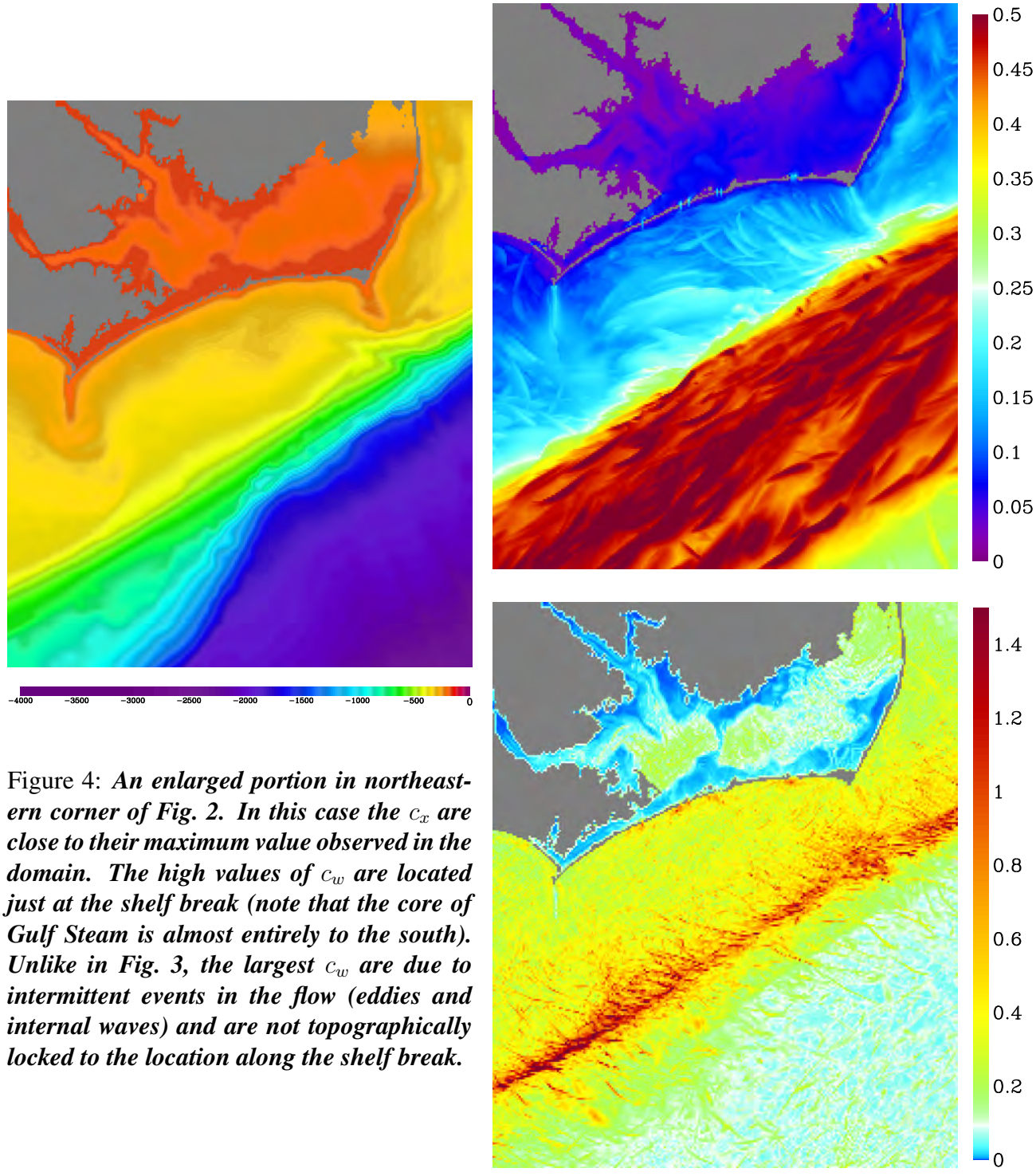

Figure 4: ***An enlarged portion in northeastern corner of Fig. 2. In this case the c_x are close to their maximum value observed in the domain. The high values of c_w are located just at the shelf break (note that the core of Gulf Steam is almost entirely to the south). Unlike in Fig. 3, the largest c_w are due to intermittent events in the flow (eddies and internal waves) and are not topographically locked to the location along the shelf break.***

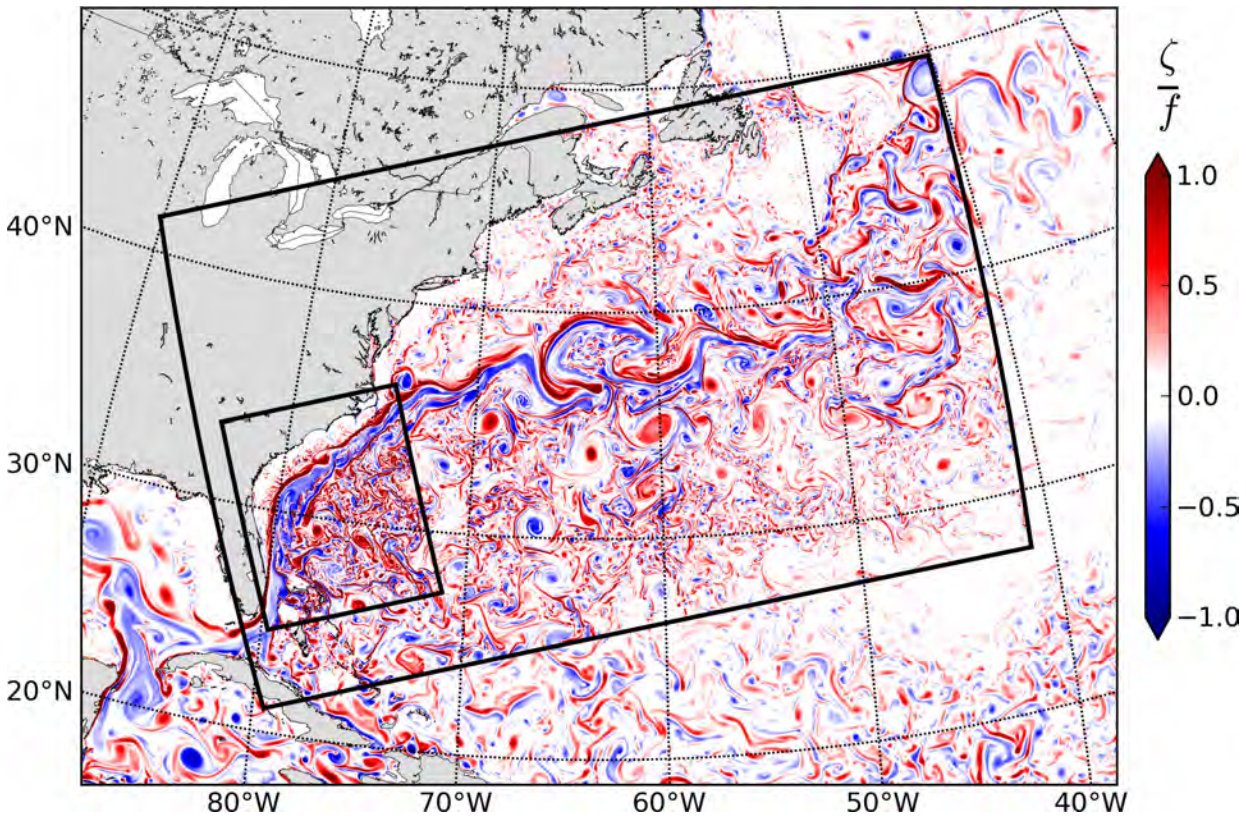

Figure 5: ***Instantaneous surface relative vorticity*** $\zeta = v_x - u_y$ ***(normalized by*** f***) in the region of the Gulf Stream at the end of winter. The boundaries of the successive nested domains at*** $\Delta x = 2.5$***km and*** $\Delta x = 750$***m are delineated by black lines. The relative vorticity inside each of the domains is computed using data at the corresponding resolution. The successive levels of grid refinement spontaneously exhibit an increasingly realistic amount of submesoscale activity.***

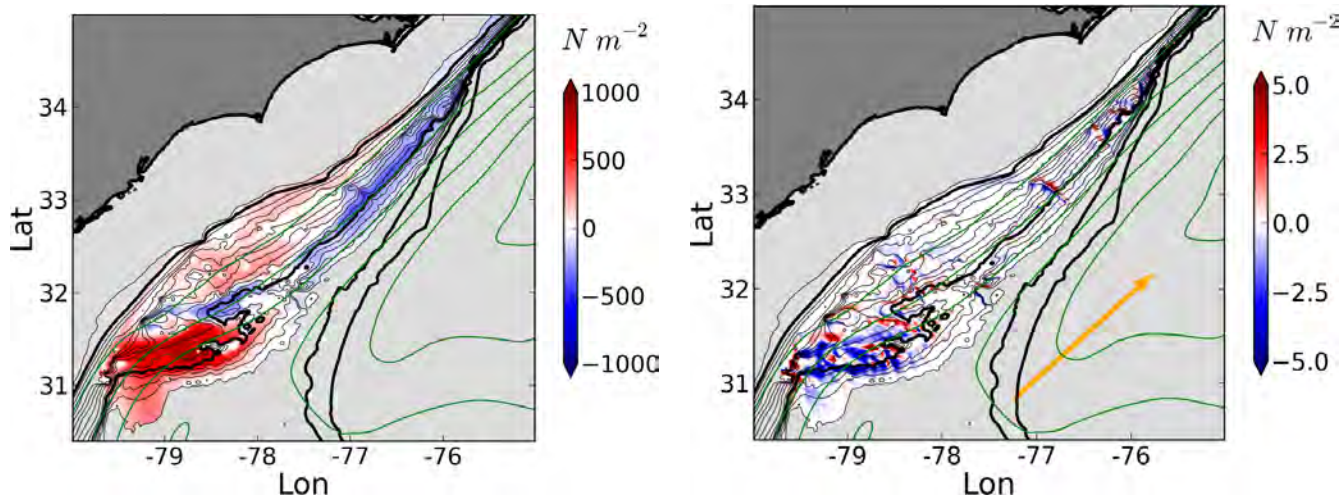

Figure 6: ***Mean bottom pressure anomaly (left) and form drag contribution along the direction of the flow (right) over the Charleston Bump area. Topography is shown in thick black contours at 0 m, 200 m, 600 m, 1000 m, and 2000 m isobaths, and in thin black contours every*** 50 ***m between 100 m and 800 m.***

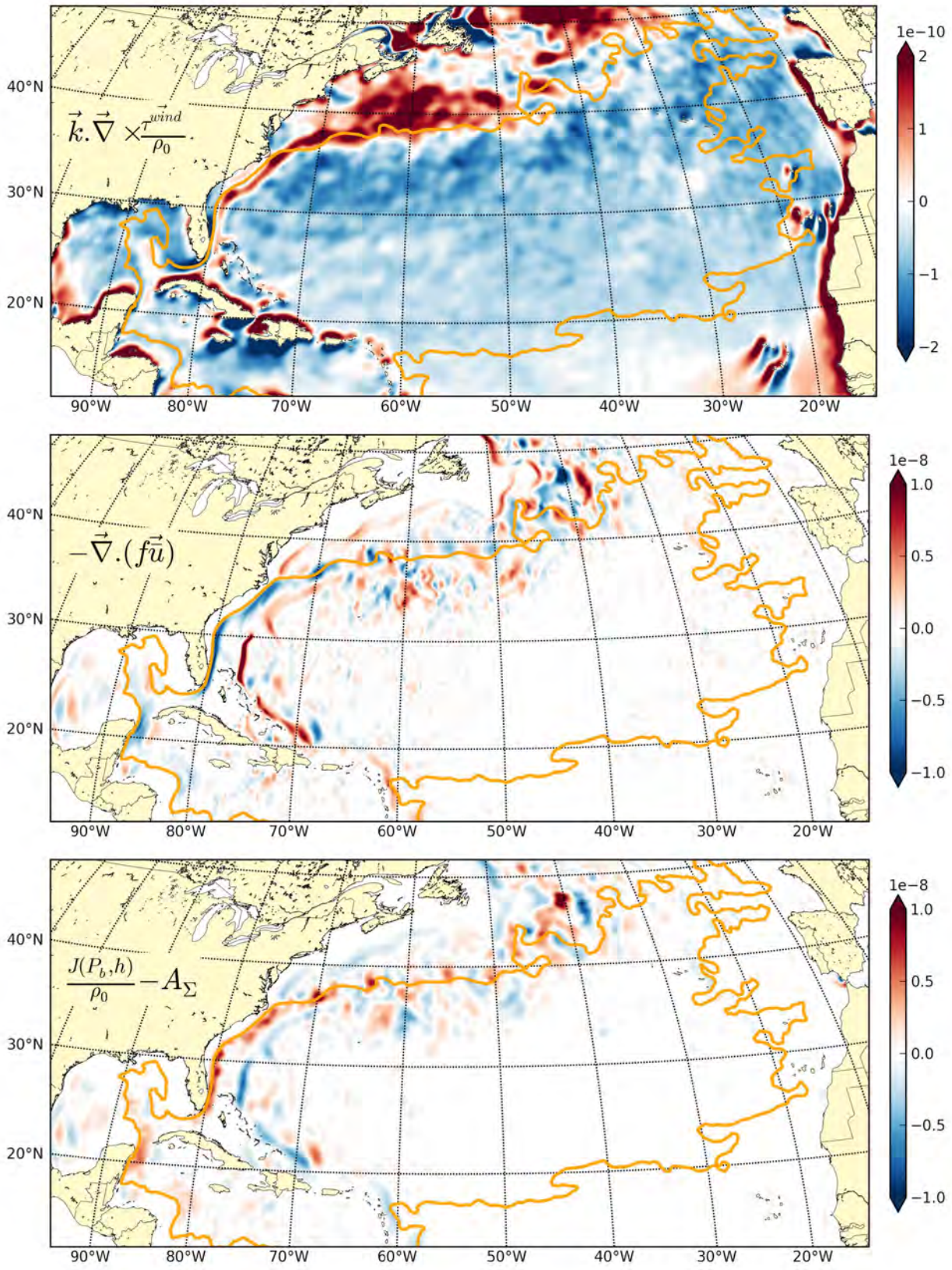

Figure 7: ***Wind stress curl*** $\vec{k}.\vec{\nabla} \times \frac{\vec{\tau^{wind}}}{\rho_0}$ ***(top), planetary vorticity term*** $-\vec{\nabla}.(f\vec{u})$ ***(middle), and sum of the bottom pressure torque and non-linear advective terms*** $J(P_b,h)/\rho_0 - A_\Sigma$***. Units are m*** s^{-2}***. The orange contour shows the*** $\Psi = 0$ ***Sv line used to define the gyre as the largest closed streamfunction contour.***

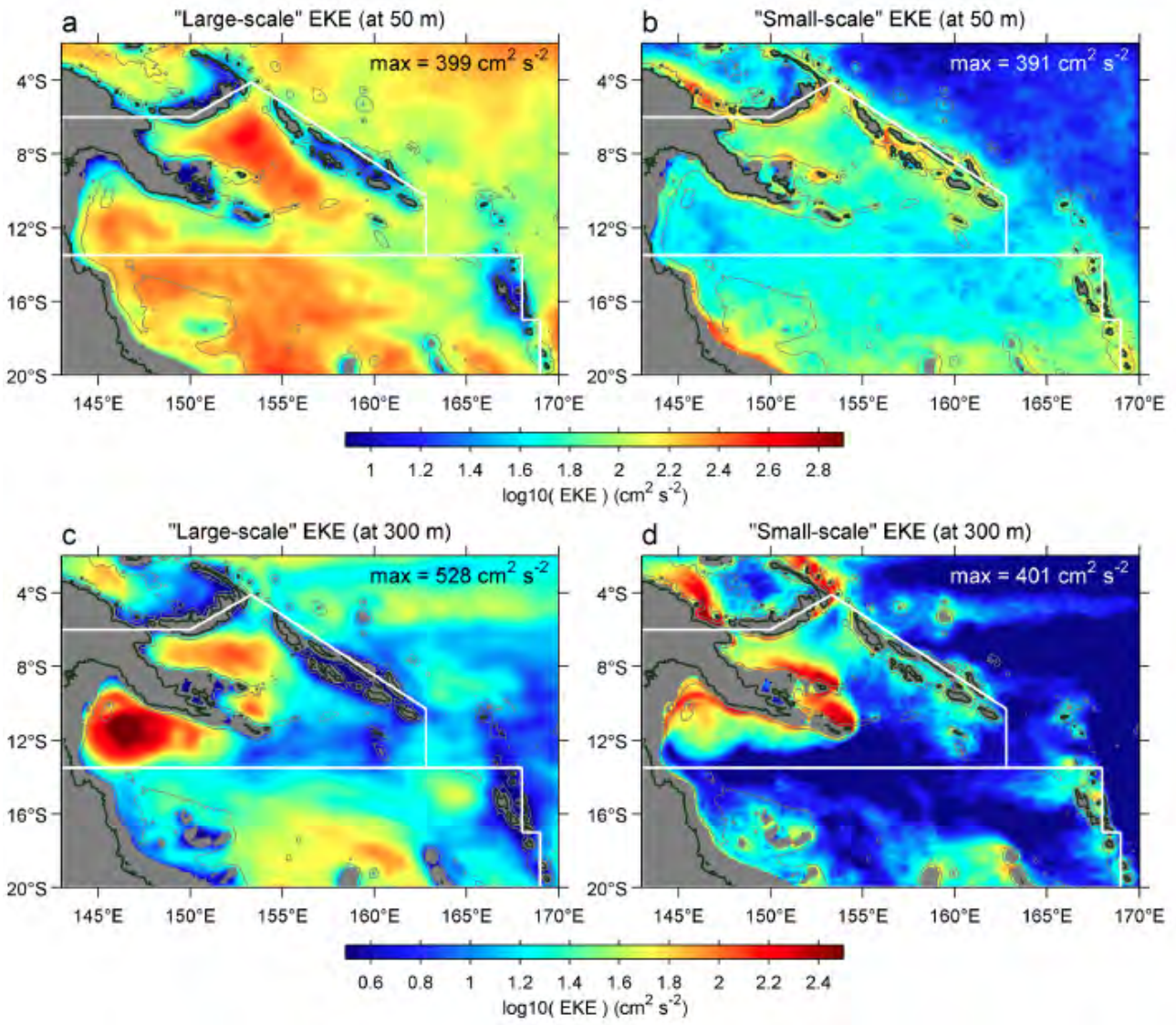

Figure 8: Mean model eddy kinetic energy (EKE) in the Southwest Pacific from a simulation with grid spacing $dx = 4$ km. EKE is plotted with a logarithmic scale: (a,b) near surface at 50 m, and (c,d) subsurface at 300 m. At each depth, EKE is split into large-scale and small-scale by spatially filtering the velocity anomalies with a horizontal scale partition of about 80 km (comparable to the resolution of satellite altimetry). The color bar limits differ between the surface and subsurface pair of plots but in both cases they span exactly 2 orders of magnitude. Notice the concentration of large-scale, subsurface EKE near the Western Boundary Current in the Gulf of Papua and south of New Britain Island and of small-scale EKE near the lateral boundaries, suggesting topographic generation. (From Hristova *et al.*, 2014)

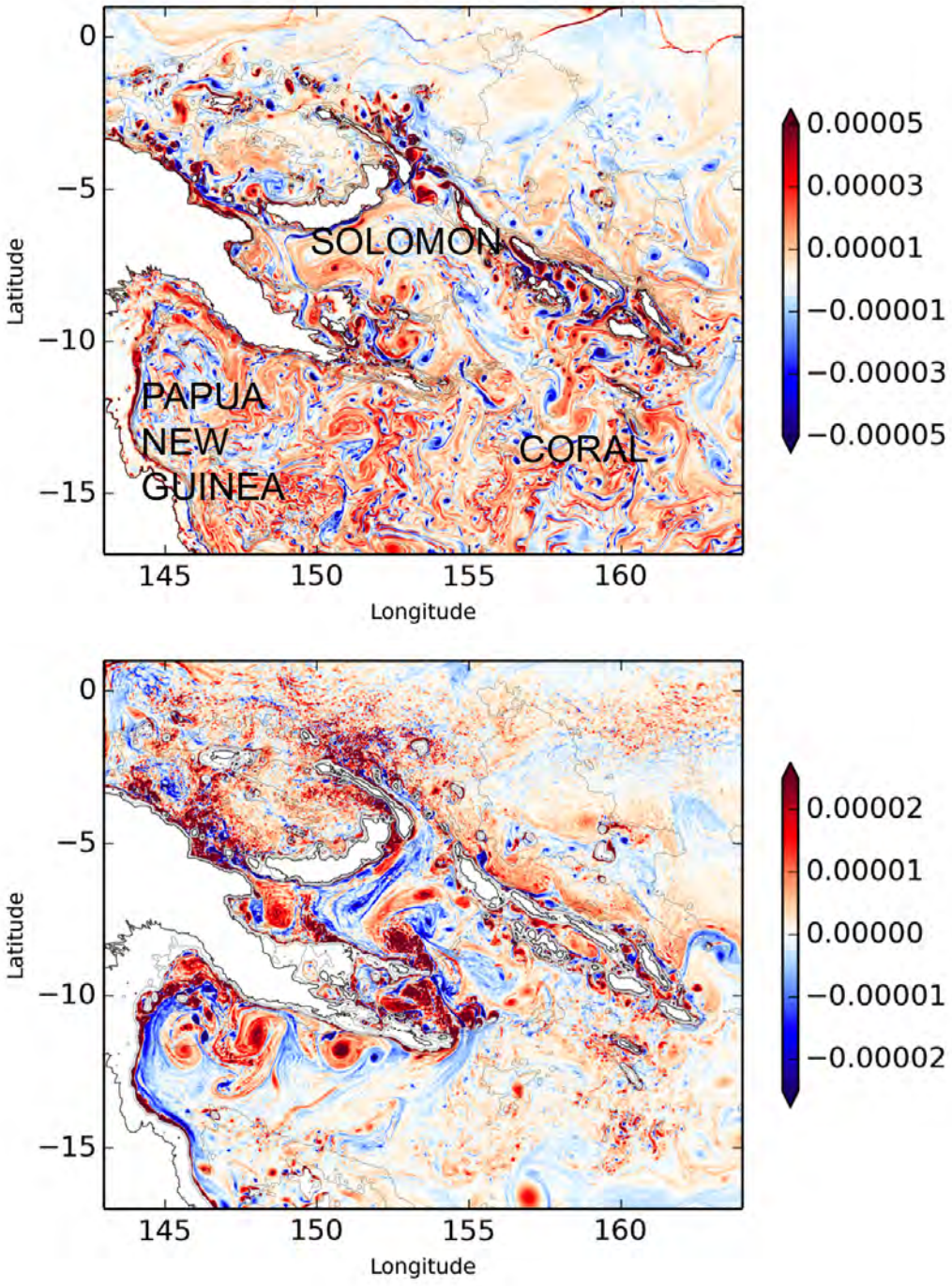

Figure 9: Relative vorticity at the surface (top) and at 500 m depth (bottom) from a $dx = 1.5$ km nested simulation of the Southwest Pacific. There are three main sub-regions. The Coral Sea is characterized by a classic surface boundary layer submesoscale activity that is likely created by mesoscale strain fields that explosively sharpen lateral buoyancy gradients. The New Guinea Western Boundary Current becomes strongly unstable when flowing across the Gulf of Papua New Guinea and the Solomon Sea due to topography interactions, generating fronts, filaments, and coherent vortices at surface and at depth. The turbulent submesoscale activity is further increased by the strong vorticity generation in the boundary layer along the complex topography of the Solomon Sea.

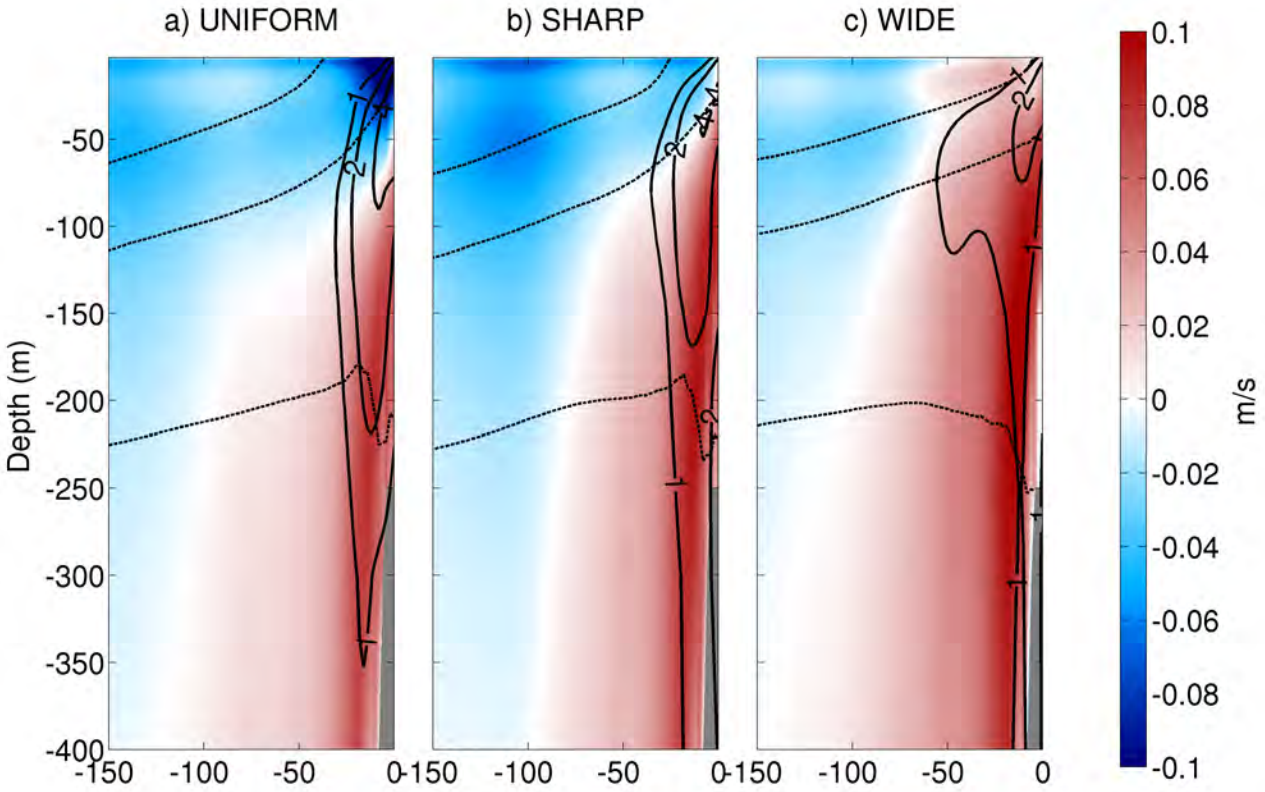

Figure 10: Cross-shore section for the California Current System between 35N and 40N during Spring for the wind drop-off sensitivity experiments. The color fields represent the alongshore current, the full contour line the vertical velocities (one contour each 2 m s^{-1}) and the dashed contour lines the temperature. For clarity, only the [10 12 14] C isotherms are shown. With a wide drop-off, the Undercurrent is stronger and the surface current can be reversed. The vertical velocities have a cross-shore re-partition that depends on the Ekman pumping and coastal upwelling.

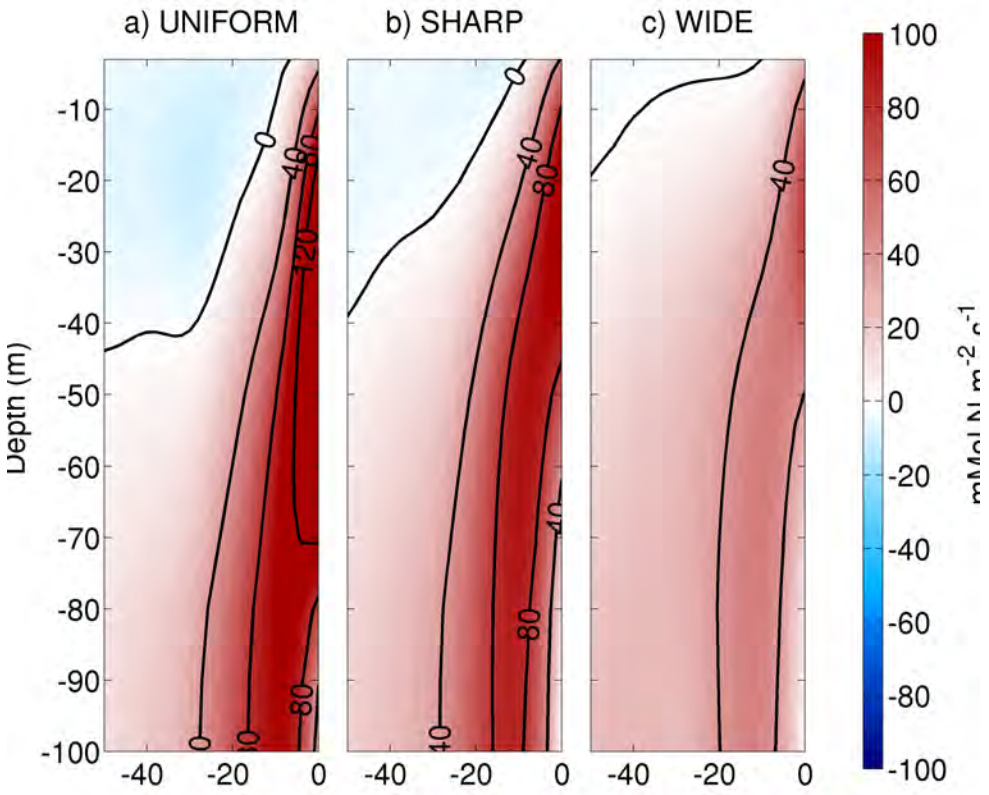

Figure 11: Nitrate vertical flux between 35N and 40N during Spring for the three wind drop-off sensitivity experiments. The different cross-shore distributions of the vertical velocity draw from a different sub-surface reservoir of Nitrate.

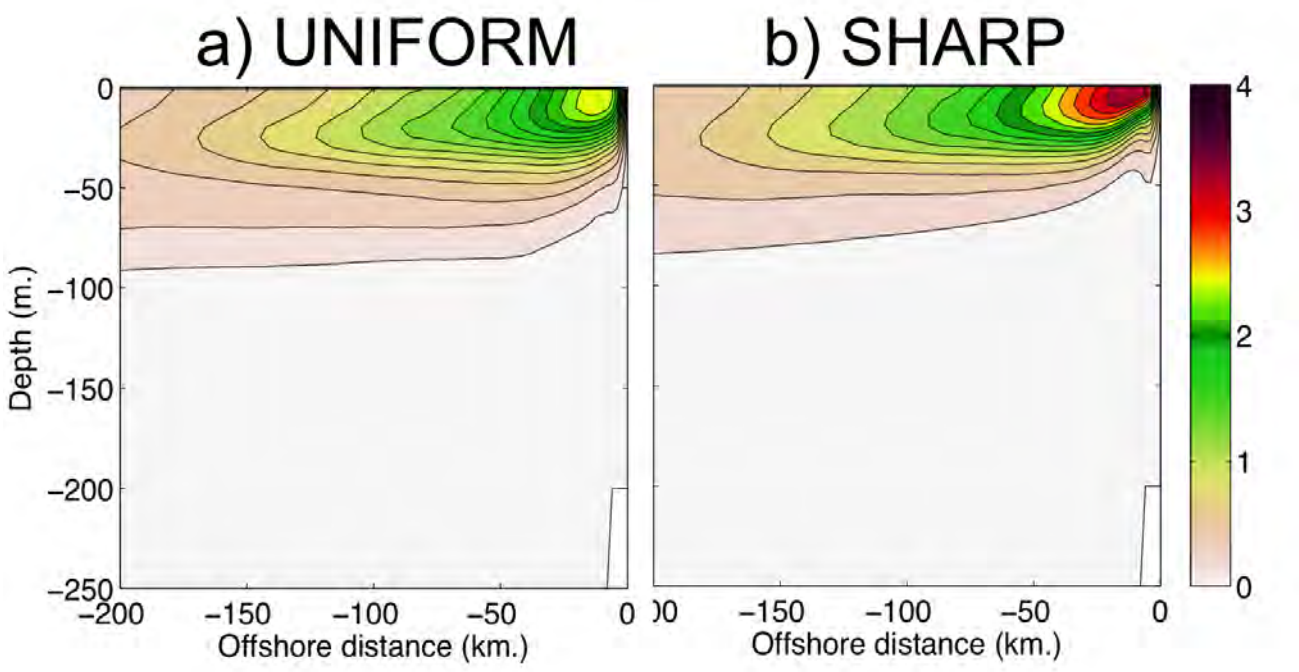

Figure 12: Mean Chlorophyll [mg m^{-3}] between 35N and 40N during Spring for two wind drop-off experiments: one with no coastal drop-off and another with a sharp drop-off width. The Primary Production can double depending on the coastal wind shape.